

See discussions, stats, and author profiles for this publication at: <https://www.researchgate.net/publication/260642756>

# Fine Refinement of Solid-State Molecular Structures of Leu- and Met-Enkephalins by NMR Crystallography

ARTICLE in THE JOURNAL OF PHYSICAL CHEMISTRY B · MARCH 2014

Impact Factor: 3.3 · DOI: 10.1021/jp500379e · Source: PubMed

---

CITATIONS

4

---

READS

7

## 2 AUTHORS, INCLUDING:



Tomasz Pawlak

Centre of Molecular and Macromolecular Stud...

25 PUBLICATIONS 162 CITATIONS

[SEE PROFILE](#)

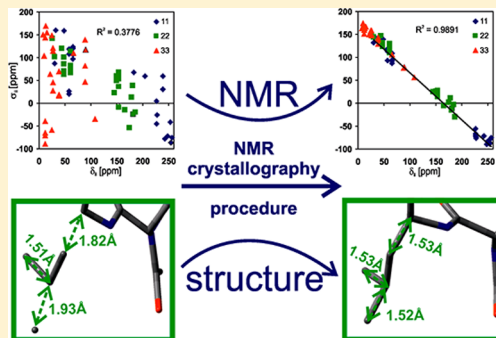
# Fine Refinement of Solid-State Molecular Structures of Leu- and Met-Enkephalins by NMR Crystallography

Tomasz Pawlak\* and Marek J. Potrzebowski\*

Centre of Molecular and Macromolecular Studies, Polish Academy of Sciences, Sienkiewicza 112, 90-363 Lodz, Poland

## S Supporting Information

**ABSTRACT:** This paper presents a methodology that allows the fine refinement of the crystal and molecular structure for compounds for which the data deposited in the crystallographic bases are of poor quality. Such species belong to the group of samples with molecular disorder. In the Cambridge Crystallographic Data Center (CCDC), there are approximately 22 000 deposited structures with an *R*-factor over 10. The powerful methodology we present employs crystal data for Leu-enkephalin (two crystallographic forms) with *R*-factor values of 14.0 and 8.9 and for Met-enkephalin (one form) with an *R*-factor of 10.5. NMR crystallography was employed in testing the X-ray data and the quality of the structure refinement. The GIPAW (gauge invariant projector augmented wave) method was used to optimize the coordinates of the enkephalins and to compute NMR parameters. As we reveal, this complementary approach makes it possible to generate a reasonable set of new coordinates that better correlate to real samples. This methodology is general and can be employed in the study of each compound possessing magnetically active nuclei.



## INTRODUCTION

Traditionally, the structural characterization of crystalline solids has been the domain of X-ray or neutron diffraction methods.<sup>1</sup> Diffraction techniques are a major source of information about crystal and molecular structures, intra- and intermolecular interactions, and long-range order for well-organized condensed matter. Unfortunately, the applicability of the methods under discussion is limited in some cases. As a result, situations occur in which the quality of the crystals used for measurements is not sufficient to provide fine refinement of the structure or when crystals in bulk undergo complex physical and/or chemical processes, leading to the arbitrary selection of a representative material. Under these circumstances, the strategy based on NMR crystallography can be useful. NMR crystallography is a relatively new approach that appeared in the literature recently. At the heart of this methodology is solid-state NMR (SS NMR), which can be combined with advanced quantum mechanical calculations to support diffraction techniques in the precise refinement of solid materials.<sup>2</sup>

Solid-state NMR is a source of structural constraints, which are extremely useful in the analysis of condensed matter. First, spectra provide a “fingerprint” of the local structure and show the local electronic environment for each nucleus under investigation. NMR responds to the short-range environments of relevant atoms and is not directly influenced by long-range order. Chemical shift is the most important NMR parameter and gives information about intermolecular interactions. The analysis of principal elements of chemical shift tensor  $\delta_{ii}$  provides detailed information about the electronic distribution around each individual nucleus. Inter- and intramolecular

hydrogen-bond linkages can be identified, and information on crystallographic asymmetric units especially is readily available, usually by merely counting lines. Polymorphs are usually easily distinguished, and phase transitions can be monitored. Crystallographic disorder is detectable, and distinctions between spatial and temporal disorder can be made. Finally, the measurement of dipolar coupling constants yields through-space interatomic (i.e., internuclear) distances, although this will be modulated by local mobility.

A number of spectacular applications of NMR crystallography in structural studies of small molecules, mostly pharmaceuticals, have been published thus far by Emsley, Brown, Harris<sup>3–10</sup> and others.<sup>11–15</sup> In our recent paper, we demonstrated the power of this methodology in the analysis of the N-terminal sequence of dermorphin, which belongs to a group of opioid peptides that interact with G-protein-coupled receptors (GPCRs).<sup>16</sup>

Our continued interest in the study of GPCR ligands and the analysis of problems related to molecular disorder for this class of solid-state compounds led us to the current work, in which we report our study of the naturally occurring enkephalins (Tyr-Gly-Gly-Phe-Leu **1** and Tyr-Gly-Gly-Phe-Met **2**), which were first found in the pig brain.<sup>17,18</sup> Enkephalins have been suggested to interact with membranes through their side chains and to undergo further conformational changes that are suitable for binding  $\delta$ - and  $\mu$ -opioid receptors.<sup>19</sup> The considerable

Received: January 13, 2014

Revised: March 6, 2014

Published: March 7, 2014

conformational flexibility of enkephalins was also observed in the crystal lattice. X-ray crystallographic studies<sup>20–22</sup> showed that Met- and Leu-enkephalin adopt a  $\beta$ -bend monomeric structure or exist in extended antiparallel dimer form. Their geometry depends on the solvent used during the crystallization process. Solvents can facilitate the creation of various thermodynamically stable molecular conformations of the solutes, “initiating” the formation of different solvatomorphic and/or polymorphic modifications.

Because of the poor quality of crystals and the complexity of systems, the X-ray structures of **1** and **2** were refined with average accuracy. Sample **1a** is a hydrate containing four molecules of H<sub>2</sub>O and four molecules of YGGFL in the asymmetric unit (CSD structure code, LENKPH11).<sup>22,23</sup> Sample **1b** is even more complex, containing eight H<sub>2</sub>O, eight DMF, and four YGGFL crystallographically non-equivalent molecules in the unit cell (CSD structure code, BIXNIF10).<sup>21,24</sup> The third sample, YGGFM **2**, contains eleven H<sub>2</sub>O and two pentapeptide crystallographically nonequivalent molecules in the asymmetric unit (CSD structure code, FABJIB).<sup>25</sup> The *R*-factors for **1a**, **1b**, and **2** were found to be 14.0, 8.9, and 10.5, respectively, locating these refinements in the group of samples with very high levels of distortions.

The aim of our work is to employ NMR crystallography to finely refine the solid-state molecular structures of Leu- and Met-enkephalins. As we show, this goal is achieved using an approach based on slow and very fast MAS SS NMR spectroscopy and theoretical calculations employing the CASTEP program,<sup>26,27</sup> which incorporates the spatial repetition of the unit cell inherent in crystals<sup>28</sup> and implements the gauge invariant projector augmented wave (GIPAW) method.<sup>29</sup> In this article, we present a step-by-step methodology in which isotropic chemical shifts, chemical shift tensor parameters, and data obtained from the analysis of molecular dynamics are used as structural restraints in precisely refining the peptide structures. Though we report results for peptides in this particular case, this methodology is general and can be employed in the study of each compound possessing magnetically active nuclei.

## ■ EXPERIMENTAL PROCEDURES

**Synthesis and Crystallization of Polymorphs of YGGFL and YGGFM.** YGGFL and YGGFM were synthesized by Lipopharm Company (Poland). The purity of the obtained compounds was >98%. Crystals of sample **1a** (YGGFL) were obtained by crystallization from a water/methanol (1:1) solution at 4 °C.<sup>22</sup> **1b** crystals were obtained from a water/DMF (3:2) solution by slow evaporation at 25 °C.<sup>24</sup> **2** crystals were obtained by cooling the sample in an equimolecular mixture of ethanol and water at 4 °C.<sup>25</sup>

**NMR Spectroscopy.** Solid-state cross-polarization magic angle spinning (CP/MAS) NMR and one-pulse <sup>1</sup>H MAS experiments were performed on a 600 MHz Avance III spectrometer (operating at 600.13, 150.90, and 60.81 MHz for <sup>1</sup>H, <sup>13</sup>C, and <sup>15</sup>N) equipped with a MAS probe head using 4 mm ZrO<sub>2</sub> rotors. A sample of <sup>13</sup>C, <sup>15</sup>N-labeled histidine hydrochloride was used to set the Hartmann–Hahn condition for <sup>13</sup>C and <sup>15</sup>N. The conventional <sup>13</sup>C CP/MAS spectra were obtained with a proton 90° pulse length of 4  $\mu$ s, a contact time of 2 ms, a repetition delay of 5 s, a spectral width of 40 kHz, and a time domain size of 3.5K data points. The acquisition data were collected with a SPINAL decoupling sequence.<sup>30</sup>

A 5- $\pi$  pulse 2D PASS scheme and 1500 and 4000 Hz sample spinning speeds were used in the 2D experiments. The  $\pi$ -pulse length was 8  $\mu$ s. Sixteen  $t_1$  increments using the timings described by Levitt et al. were used in the 2D PASS experiments.<sup>31</sup> For each increment, 360 scans were collected. Because the pulse positions in the  $t_1$  set returned to their original positions after a full cycle and the  $t_1$ -FID formed a full echo, the 16-point experimental  $t_1$  data were replicated to 256 points. Acquisition time was 18 h. After the Fourier transformation in the direct dimension, the 2D spectrum was sheared to align all side bands with the center bands in the indirect dimension of the 2D spectrum. One-dimensional chemical shift anisotropy (CSA) spinning sideband patterns were obtained from  $t_1$  slices taken at the isotropic chemical shifts in the  $t_2$  dimension of the 2D spectrum. The values of the principal elements of the CSA tensor were obtained from the best-fit simulated spinning sideband pattern. Simulations of the spinning CSA sideband spectra were performed on a PC using the Bruker TopSpin 3.0 program.<sup>32</sup>

The PISEMA MAS experiment<sup>33</sup> was carried out with an <sup>1</sup>H effective field strength of 50 kHz in all of the experiments, and the <sup>13</sup>C spin-lock field strengths were adjusted to the first-order sideband condition,  $\omega_{13\text{C}} = \omega_{1\text{Heff}} \pm \omega_r$ . The spinning speed was 13 kHz and was regulated to  $\pm 3$  Hz by a pneumatic control unit. The spectra were acquired in 64 rows, with 512 scans per row and a recycle delay of 3 s. The acquisition time was 28 h. The 2D PISEMA MAS experiments incremented the SEMA contact time using a step of 16.28  $\mu$ s. At a spinning speed of 13 kHz, the dwell time for the evolution period was 19.23  $\mu$ s. The maximum  $t_1$  evolution time was approximately 1 ms. Only cosine-modulated data were collected. Thus, a real Fourier transformation was performed on the  $t_1$  data that yielded spectra with a symmetrized  $\omega_1$  dimension and dipolar splitting. Because the  $t_1$  time signal increases with increasing SEMA contact time, the  $\omega_1$  dimension was processed using the baseline correction mode “qfil” in the Bruker TopSpin 3.0 program software, which subtracted a constant intensity from the time signals prior to the Fourier transformation and yielded spectra free from the dominant zero-frequency peak that gives the <sup>1</sup>H–<sup>13</sup>C doublet.

The solid-state very fast MAS spectra with spin rates up to 60 kHz (with a very fast broad band CP/MAS probe head using 1.3 mm ZrO<sub>2</sub> rotors) were recorded on a 600 MHz Avance III spectrometer. A sample of <sup>13</sup>C, <sup>15</sup>N-labeled histidine hydrochloride was used to set the Hartmann–Hahn condition for <sup>13</sup>C and <sup>15</sup>N. The one-pulse <sup>1</sup>H MAS was performed at a 60 kHz spin rate with a proton 90° pulse length of 2.5  $\mu$ s, a repetition delay of 3 s, a spectral width of 36 kHz, and a time domain size of 8K data points. The <sup>1</sup>H–<sup>13</sup>C HETCOR (for indirect detection of <sup>13</sup>C) experiments were performed using the pulse sequence described by Mao et al.<sup>34</sup> The following parameters were used: a 60 kHz spin rate, a proton 90° pulse length of 2.5  $\mu$ s, a first contact time of 2 ms, a second contact time of 2 ms or 200  $\mu$ s, and a proton  $\pi$  pulse (5  $\mu$ s) in the middle of the evolution period (instead of CW <sup>1</sup>H decoupling as mentioned by Ishii and Tycko).<sup>35</sup> The maximal evolution times were  $T_{1\text{max}} = 4.2$  ms and  $T_{2\text{max}} = 20$  ms. The spectra were acquired in 180 rows, with 128 scans per row and acquisition time of 20 h.

The <sup>1</sup>H–<sup>15</sup>N HETCOR experiments were conducted using the same pulse sequence as in the case of <sup>1</sup>H–<sup>13</sup>C HETCOR. The maximal evolution times were  $T_{1\text{max}} = 6.4$  ms and  $T_{2\text{max}} = 60$  ms. The spectra were acquired in 128 rows, with 560 scans per

row and acquisition time of 60 h. All data were processed using the Bruker TopSpin 3.0 program.<sup>32</sup>

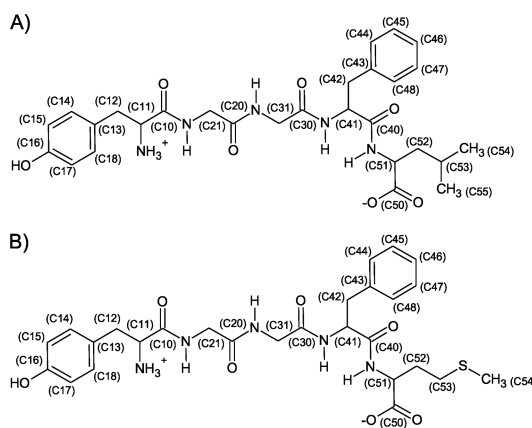
Adamantane (resonances at 38.48 and 29.46 ppm) was used as a secondary <sup>13</sup>C chemical-shift reference from external tetramethylsilane (TMS) in all experiments.<sup>36</sup> <sup>15</sup>N chemical shift was referenced indirectly to neat liquid ammonia by using powdered <sup>15</sup>N glycine as an external secondary referenced  $\delta = 34.10$  ppm.

**QM Calculations. DFT Calculations in Periodic Boundary Conditions.** The quantum chemical calculations were performed using the CASTEP<sup>27</sup> code. The geometry optimization was performed using the X-ray diffraction crystal structures of **1a** (LENKPH11),<sup>22</sup> **1b** (BIXNIF10),<sup>24</sup> and **2** (FABJIB)<sup>25</sup> as an input file, and the generalized density approximation DFT functional PBE<sup>37</sup> was applied. A comparison of the average forces remaining on the atoms after geometry optimization was carried out for proton-only and all-atom optimizations by using a maximum plane wave cutoff energy of 550 eV and ultrasoft pseudopotential.<sup>38</sup> We observed average forces (given as Cartesian components) of approximately 0.003 eV/Å (protons), 1.600 eV/Å (carbons), 0.750 eV/Å (nitrogens), and 0.650 eV/Å (oxygens) after proton-only optimization of all analyzed structures which suggested that proton-only optimized structures are not the most preferable structure at the considered level of theory. After all-atom optimizations the average forces were smaller (especially for heavy atoms), with similar magnitude for all atomic species, that is, approximately 0.002 eV/Å (protons), 0.004 eV/Å (carbons), 0.004 eV/Å (nitrogens), and 0.007 eV/Å (oxygens), which clearly indicated that these structures are much more preferable. The unit cell parameters were taken from the X-ray structures and kept fixed during the optimization of the geometry of the structures, and a Monkhorst–Pack grid<sup>39</sup> was used to sample the Brillouin zone. The total number of atoms in unit cell was 652, 856, and 366 for structures **1a**, **1b**, and **2**, respectively. The NMR chemical shifts were computed using the GIPAW method. When the full crystal structure was calculated, a plane wave basis set with a maximum cutoff energy of 550 eV was used. Finally, we obtained NMR chemical-shielding values in periodic boundary conditions using two approaches: (i) optimized with only the hydrogen atoms allowed to relax and (ii) optimized so that all atoms were allowed to relax. In all cases, the optimization algorithm was BFSG<sup>40</sup> with line search. All numerical data are presented in the Supporting Information.

## RESULTS AND DISCUSSION

**(i) Precise Assignment of the <sup>13</sup>C Chemical Shifts for Crystals **1a** and **1b**.** The X-ray data for two forms of YGGFL (**1a** and **1b**) and YGGFM (**2**) have been reported.<sup>22,24,25</sup> Scheme 1 shows the primary structure and numbering system for both enkephalins. The molecular packing is displayed in Figure 1. The unit cell volumes of **1a**, **1b**, and **2** are 13501.1, 8462.5, and 3447.9 Å<sup>3</sup>. Such a large unit cell size is not very common for peptides, although some have been observed in a few cases reported elsewhere.<sup>41</sup> The conformation of the peptide backbone is strongly influenced by the solvent used during crystallization. **1a** creates a pseudocyclic conformation with one intermolecular hydrogen bond, whereas structures **1b** and **2** represent rather linear conformations. For all three crystals, the number of strong intermolecular hydrogen bonds between the solvent and peptide molecules and the antiparallel orientation of the phenylalanine and tyrosine aromatic ring along the peptide backbone are observed.

**Scheme 1. Molecular Structures and Numbering Systems of (A) YGGFL and (B) YGGFM**



The <sup>13</sup>C CP/MAS spectra of **1a**, **1b**, and **2** were recorded at ambient temperature with a spinning rate of 12 kHz and are shown in Figure 2. The literature reporting NMR signal assignments to the solid-state molecular structures of enkephalins is very limited. The preliminary analysis of <sup>13</sup>C SS NMR spectra was reported by Saito et al.<sup>42,43</sup> The major difficulty in interpreting the data is the insufficient dispersion of diagnostic resonances. In many cases, the crystallographically nonequivalent positions in the asymmetric unit cell are magnetically equivalent. For the most complex case of **1b**, which consists of four molecules in the asymmetric unit (labeled as A, B, C, and D), the <sup>13</sup>C signals overlap. Thus, the full assignment of signals shown in Figure 2 is ambiguous. Advanced theoretical calculations can be employed to make a reasonable assignment. The details regarding the employed computing method of computing will be discussed in section v.

**(ii) Assignment of <sup>1</sup>H Signals by Very Fast MAS NMR and <sup>1</sup>H–<sup>13</sup>C and <sup>1</sup>H–<sup>15</sup>N Inverse HETCOR (Inv-HETCOR) MAS 2D NMR Correlations.** One of the most important structural parameters in NMR spectroscopy is the isotropic chemical shifts of protons, which are very sensitive to the local electronic environment.<sup>44</sup> The <sup>1</sup>H  $\delta_{\text{iso}}$  are usually valuable constraints that can be further used in theoretical calculations for structure prediction. Unfortunately, the assignment of the <sup>1</sup>H resonances and quantitative analysis of spectra in the solid state remain very challenging because of the extremely strong homonuclear dipolar couplings, which in many cases exceed the range of chemical shifts for protons. For true solids, the broadening of proton lines is not prevented by slow or medium magnetic angle spinning without the application of complex pulse sequences.<sup>45,46</sup> Spectra recorded under slow conditions are therefore difficult to analyze, and they usually do not contain subtle structural information.

Under a “very fast” (VF) spinning regime exceeding 50 kHz, which can be obtained using commercially available 1.3 mm rotors, the spinning frequency exceeds the strength of homonuclear proton dipolar coupling and is therefore expected to enter a new regime for spin dynamics.<sup>47–49</sup> Figure 3 shows the <sup>1</sup>H VF MAS spectra of **1a**, **1b**, and **2** recorded with a spinning rate of 60 kHz at room temperature. Unfortunately, despite the very fast spinning of the samples, the spectral resolution is dissatisfying and the spectra are uninterpretable.

An alternative approach for the unambiguous assignment of proton positions in the solid state is indirect detection employing heteronuclear correlations (HETCOR). Solid-state

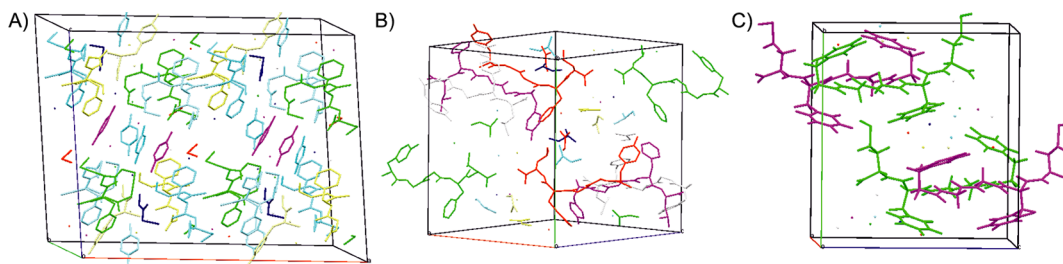


**Figure 1.** Unit cells containing (A) sixteen molecules of **1a**, (B) eight molecules of pentapeptide **1b**, and (C) four molecules of **2**. Colors represent symmetry equivalent positions.

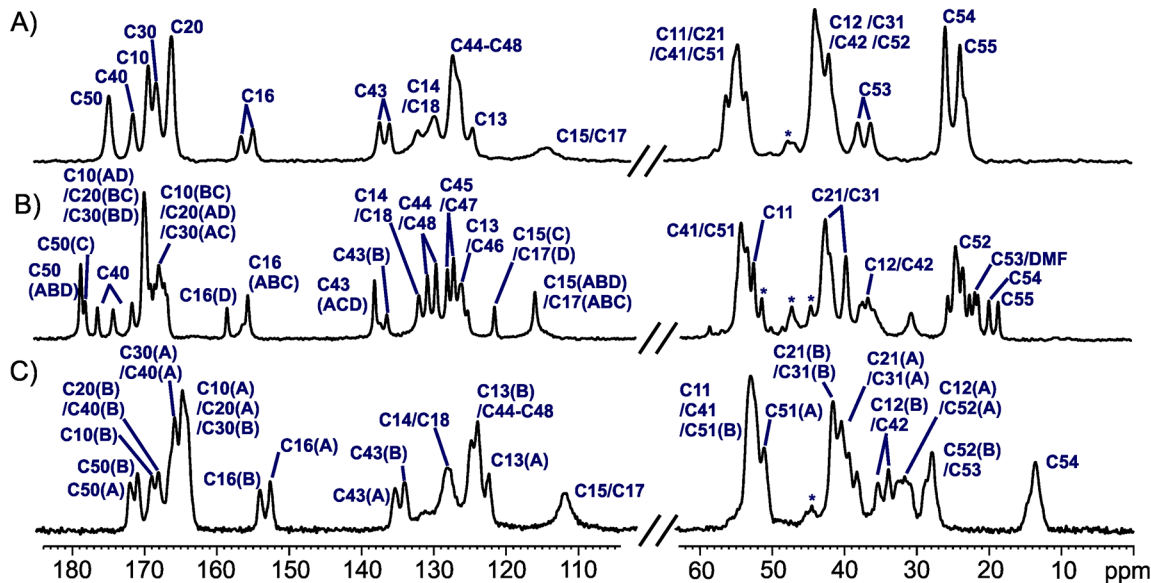


**Figure 2.** <sup>13</sup>C CP MAS NMR spectra of (A) **1a**, (B) **1b**, and (C) **2** recorded at a spinning rate of 12 kHz. The resonances are assigned by employing the GIPAW method.

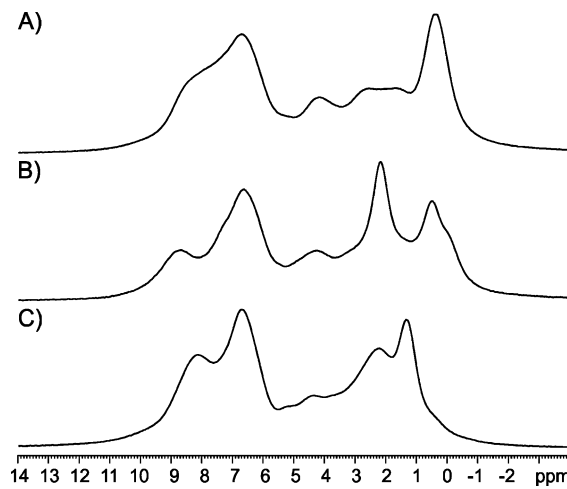


**Figure 3.** <sup>1</sup>H experimental spectra of samples **1a** (A), **1b** (B), **2** (C) recorded with a spinning rate of 60 kHz.

HETCOR spectroscopy was introduced in 1982 by Caravatti et al.<sup>50,51</sup> This methodology was greatly improved during subsequent years (e.g., frequency switched Lee–Goldburg HETCOR).<sup>52</sup> The problem of low sensitivity for such experiments, which results from the direct observation of <sup>13</sup>C nuclei, was recently solved by the application of VF MAS spectroscopy and the application of inverse <sup>1</sup>H-detected

experiments.<sup>35,53</sup> Pruski et al. have recently presented a few spectacular applications of inverse detected (Inv-HETCOR) experiments under VF MAS.<sup>54</sup> We used this methodology to assign experimental <sup>1</sup>H chemical shifts for enkephalins.

Figure 4 shows <sup>1</sup>H–<sup>13</sup>C and <sup>1</sup>H–<sup>15</sup>N Inv-HETCOR VF MAS correlations for all three models. Although the correlation peaks are quite broad, they are sufficiently separated to precisely assign signals via <sup>13</sup>C resonances (Figure 4A,C,E). The analysis of <sup>1</sup>H–<sup>15</sup>N spectra (Figure 4B,D,F) clearly shows an overlap of the <sup>1</sup>H signals of amide residues for crystallographically nonequivalent molecules in the asymmetric unit. <sup>15</sup>N resonances of the Tyr-NH<sub>3</sub> group are separated from other nitrogen residues, making the assignment of correlated protons easier. The full assignment of protons is included in the Supporting Information. The obtained chemical shifts were used in the final evaluation of the structures discussed in section vi.

### (iii) Analysis of <sup>13</sup>C Chemical Shift Tensor (CST) Parameters.

To further analyze useful parameters for the refinement of solid-state structures, we used an approach that allows us to extract values for the <sup>13</sup>C chemical shift tensor (CST) parameters. The analysis of CST for enkephalins is challenging because of the complexity of the spectra for crystals that consist of two (sample **2**) or four (samples **1a** and **1b**) crystallographically nonequivalent peptides and contain solvent molecules in the lattice. To establish <sup>13</sup>C CST parameters, we applied a 2D NMR approach. 2D PASS sequence was used

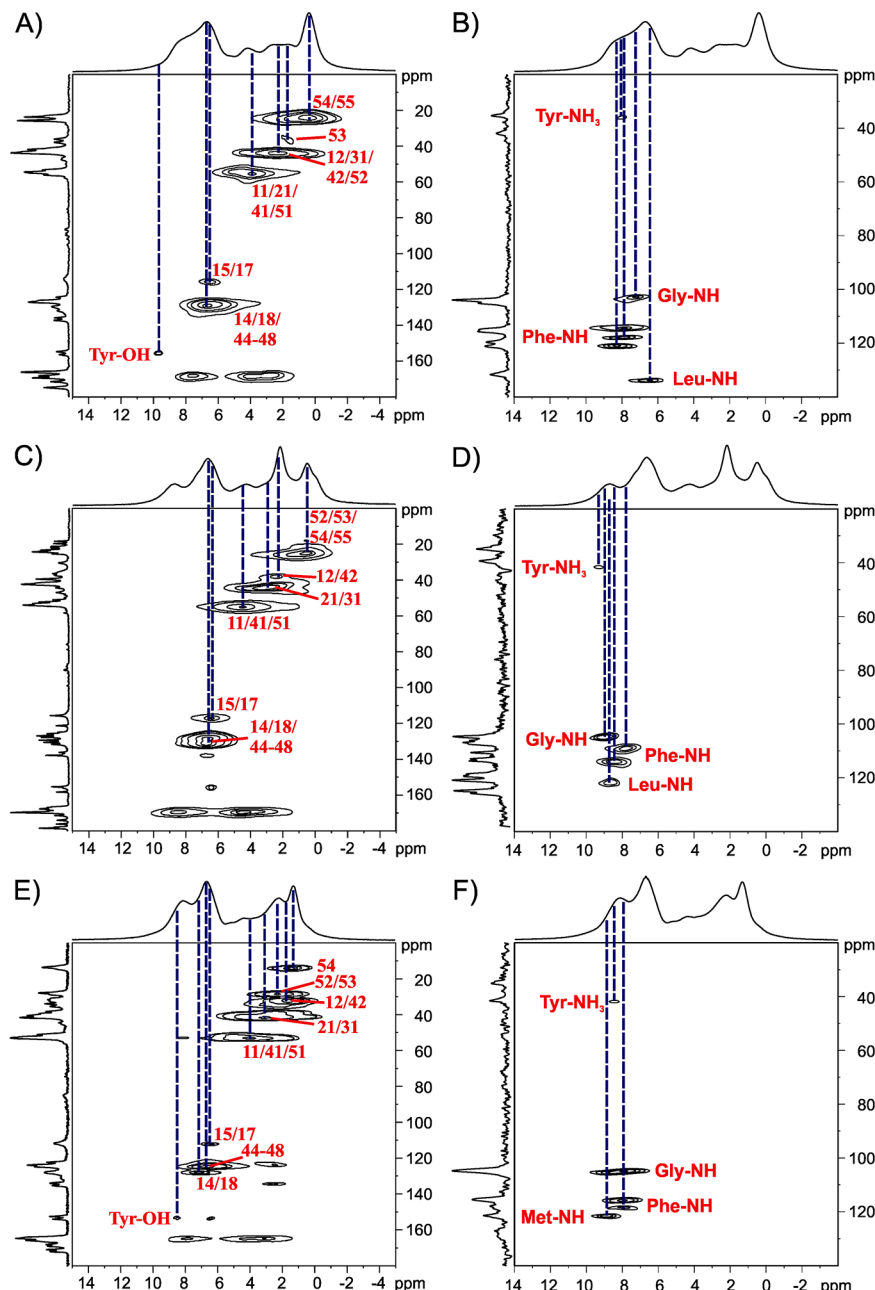


**Figure 4.**  $^1\text{H}$ - $^{13}\text{C}$  (A, C, E) and  $^1\text{H}$ - $^{15}\text{N}$  (B, D, F) inverse detected HETCOR NMR spectra acquired at a 60 kHz spinning rate and 298 K for **1a** (A, B), **1b** (C, D), and **2** (E, F). Spectra were recorded for samples with natural abundance of  $^{13}\text{C}$  and  $^{15}\text{N}$  isotopes.

because this technique offers good sensitivity without overlapping the sideband systems.<sup>31</sup> By use of proper data shearing for each nuclei, the spinning sideband systems were separated and used to assign the values of the principal elements  $^{13}\text{C}$   $\delta_{ii}$  ( $ii = 11, 22, \text{ and } 33$ ) of CST.

Figure 5 displays the 2D PASS spectrum of **1a** measured with a sample rotation of 1.5 kHz. A similar procedure was employed to study **1b** and **2**. The spectrum exhibits a complex pattern under slow sample spinning. It is clear from this presentation (Figure 5B) that the  $F_2$  projection corresponds to the TOSS spectrum,<sup>55</sup> whereas  $F_1$  represents chemical shift anisotropy (CSA). To fit the spinning sideband pattern of the  $F_1$  spectra, we employed a previously published protocol.<sup>41,56</sup> All experimental CST parameters are listed in the Supporting Information.

**(iv) Molecular Dynamics Analysis.** It is well-known that in the solid state, local molecular dynamics will average NMR tensor parameters such as the CSA, dipolar interactions, and quadrupolar interactions.<sup>56,57</sup> The quantum chemical calculations are typically performed using static structures, i.e., at 0 K where zero-point motion is neglected. As shown in recent papers, molecular dynamics can lead to significant discrepancies between computed and experimental data.<sup>56,58</sup> Thus, the knowledge about possible molecular motions in the crystal lattice is crucial for properly interpreting data.

SS NMR is an analytical technique that systematically extends the repertoire of novel approaches, allowing a better understanding of the nature of the molecular motions in condensed matter. Parameters such as  $^{13}\text{C}$  and  $^1\text{H}$  spin-lattice relaxation times ( $^{13}\text{C}$   $T_1$  and  $^1\text{H}$   $T_1$ ), carbon and proton

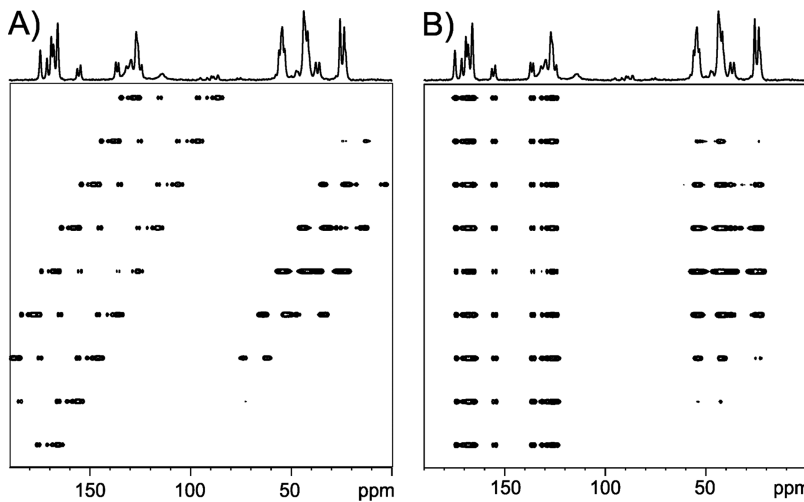


Figure 5. 2D PASS spectra for **1a** recorded with a spinning rate of 1500 Hz (A) and after data shearing (B).

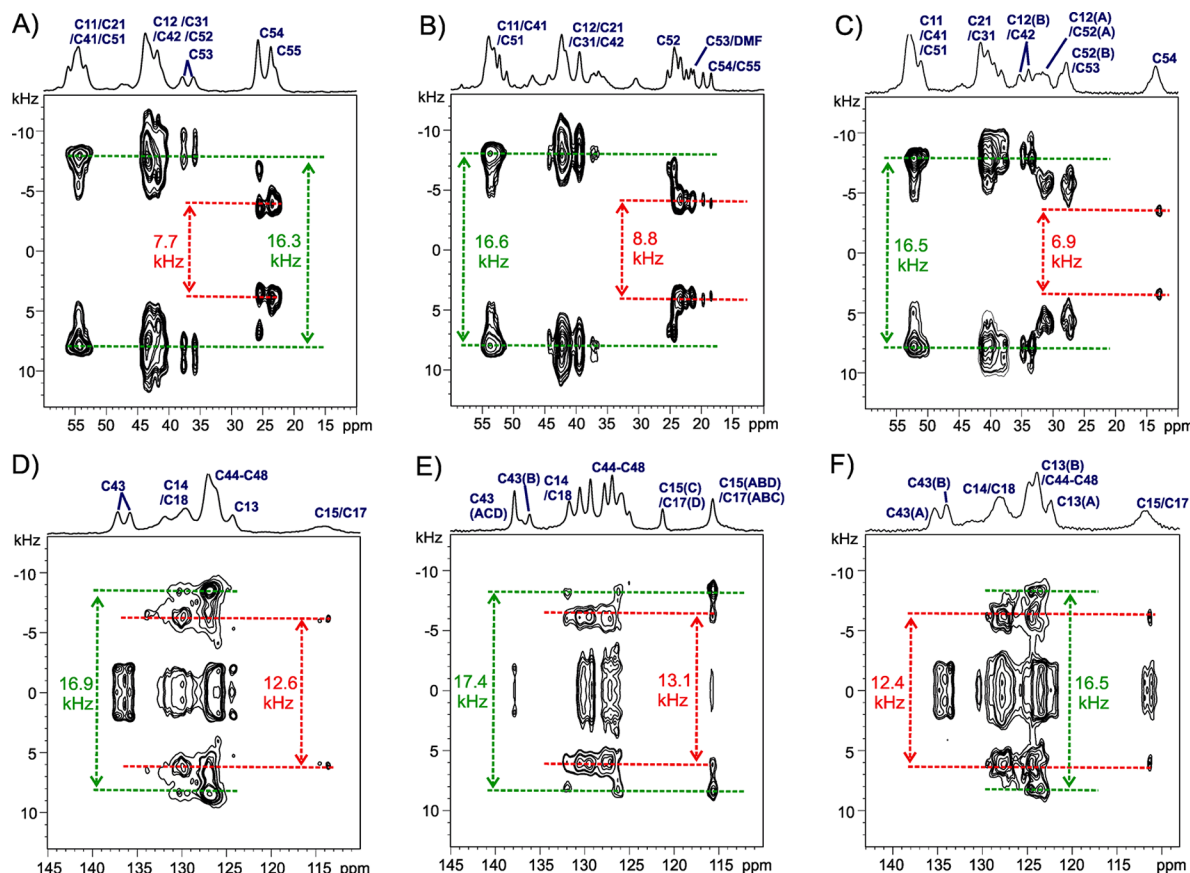
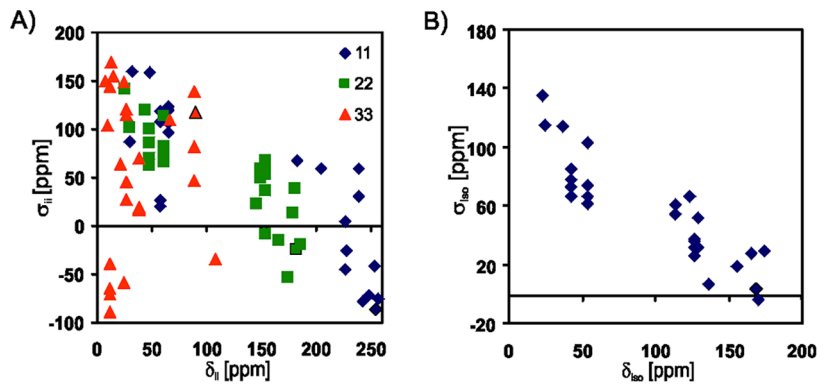


Figure 6. 2D PISEMA MAS spectra for sample **1a** (A, D), **1b** (B, E), and **2** (C, F) in the aliphatic (up) and aromatic regions (down). The highest and the lowest splitting values are labeled in each region.

rotating frame relaxation times ( $^{13}\text{C}$   $T_{1\rho}$  and  $^1\text{H}$   $T_{1\rho}$ ), the C–H cross-relaxation constant ( $T_{\text{C}-\text{H}}$ ), and the proton relaxation time in the dipolar state ( $T_{1\text{D}}$ ) exhibit substantial utility for elucidating local dynamics. Another group of techniques is based on the analysis of dipolar interactions. The partial averaging of C–H and/or N–H dipolar couplings gives either geometric information or the amplitude of the motional processes in the solid state. For the MAS approach, the measurement of heteronuclear dipolar couplings must employ recoupling techniques that efficiently reintroduce  $\text{X}^{-1}\text{H}$  ( $\text{X} =$

$^{13}\text{C}$ ,  $^{15}\text{N}$ ) dipolar interactions.<sup>59–61</sup> One substantial achievement in the field of measuring  $\text{X}^{-1}\text{H}$  dipolar couplings was the introduction of the PISEMA technique<sup>33,62</sup> and its variants, which allowed for the determination of dipolar interactions under MAS.<sup>33,63–65</sup>

Figure 6 shows 2D PISEMA MAS spectra for samples **1a**, **1b**, and **2** displayed in the form of a 2D NMR contour plot. Selected F1 slices taken from 2D NMR spectra are attached as Supporting Information. The splitting between the singularities of the doublets reflects the dipolar coupling between the proton



**Figure 7.** Correlation of experimental chemical shift tensor values ( $\delta_{ii}$ ) and calculated nuclear shielding parameters ( $\sigma_{ii}$ ) (A), as well as experimental isotropic chemical shift values ( $\delta_{iso}$ ) and calculated nuclear shielding values ( $\sigma_{iso}$ ) (B) for structure 1a.

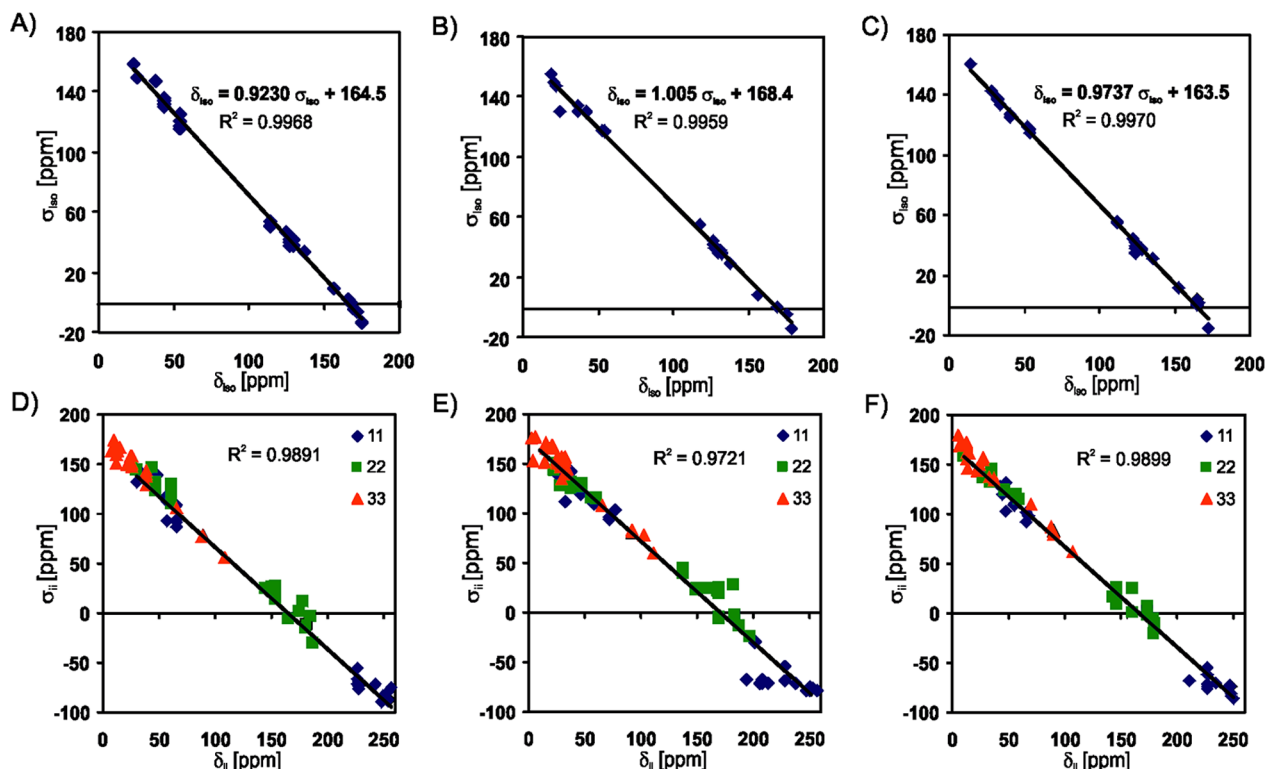


**Figure 8.** The upper plots show the correlation of experimental isotropic chemical shift values ( $\delta_{iso}$ ) and calculated nuclear shielding values ( $\sigma_{iso}$ ). The bottom plots represent the correlation of experimental chemical shift tensor values ( $\delta_{ii}$ ) and calculated nuclear shielding parameters ( $\sigma_{ii}$ ) of the enkephalin peptides. The correlations of the experimental versus the computed parameters are shown for 1a (A, D), 1b (B, E), and 2 (C, F).

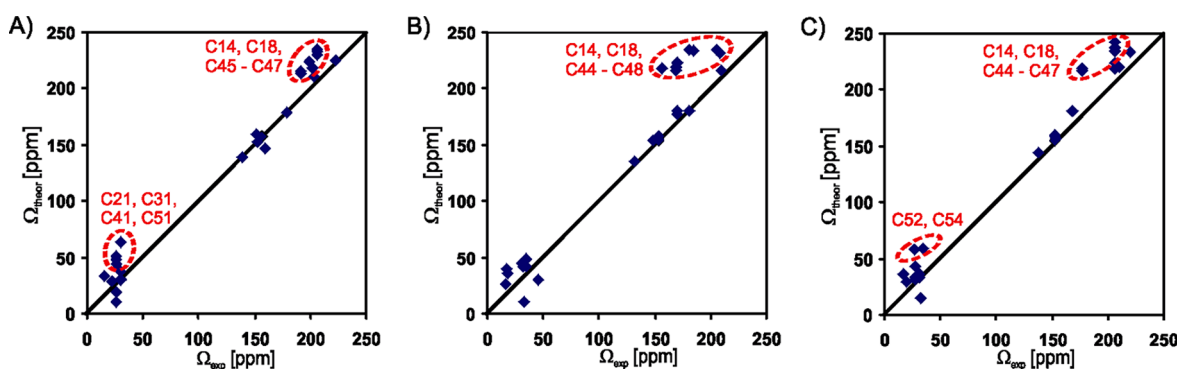


**Figure 9.** Correlations between the experimental span ( $\Omega_{exp}$ ) and calculated span values ( $\Omega_{calc}$ ) using GIPAW for samples 1a (A), 1b (B), and 2 (C). Solid lines indicate ideal correlations with a slope equal to 1.

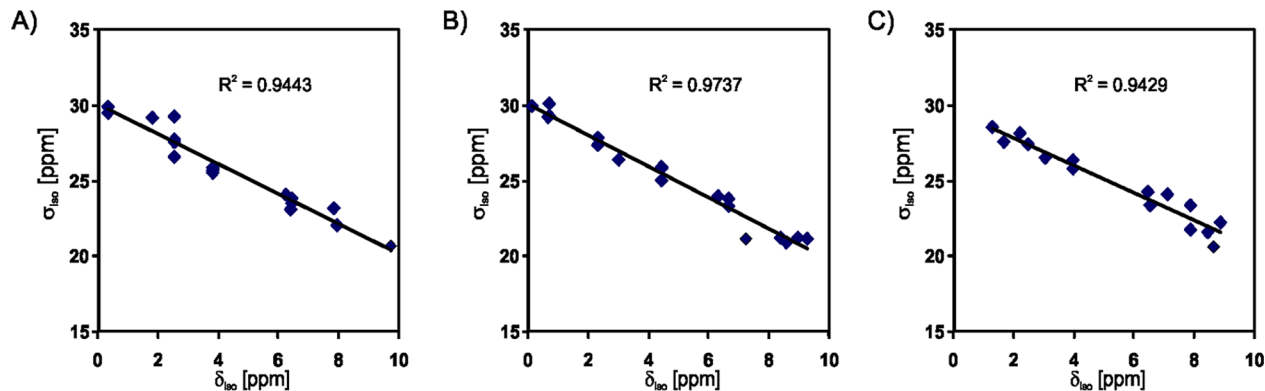


**Figure 10.** Correlations of experimental isotropic  $^1\text{H}$  chemical shift values ( $\delta_{\text{iso}}$ ) and calculated nuclear shielding values ( $\sigma_{\text{iso}}$ ) of the enkephalin peptides **1a** (A), **1b** (B), and **2** (C).

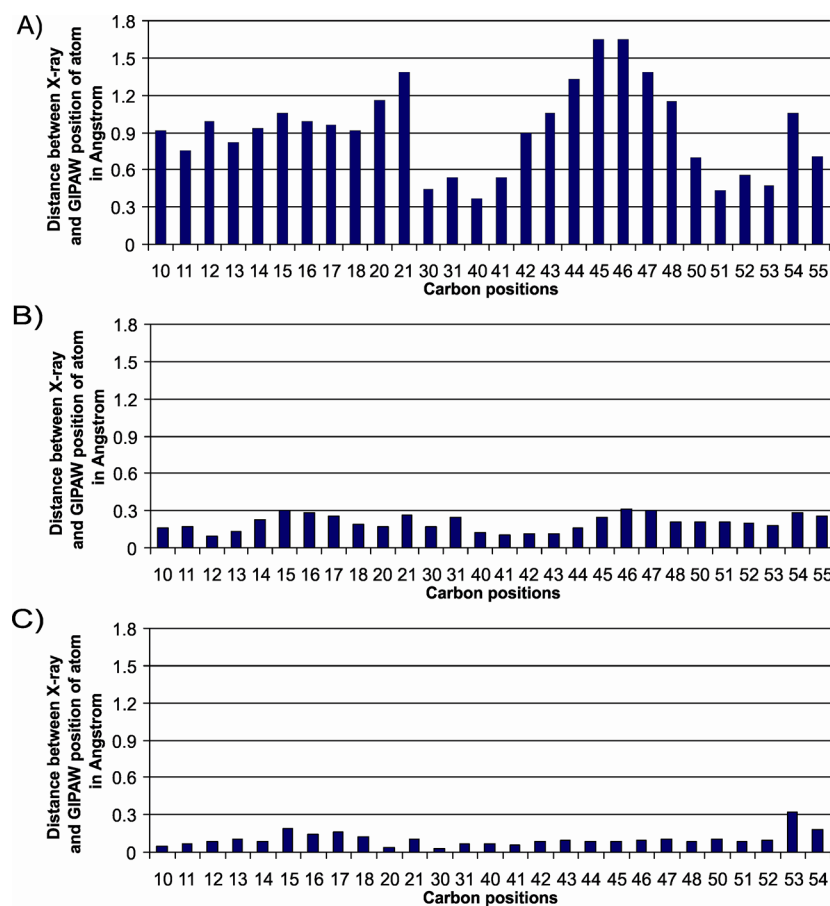


**Figure 11.** Differences in angstrom between the positions of carbon atoms determined by the X-ray and GIPAW methods for structures **1a** (A), **1b** (B), and **2** (C).

and carbon. According to the equation  $\delta = -[\mu_0/(4\pi^2)](\gamma_i\gamma_j)/r_{ij}^3$ , the dipolar coupling constant for the rigid limit for a  $^{13}\text{C}-^1\text{H}$  distance equal to 1.09 Å is 22.7 kHz. The experimentally measured splitting values are smaller than the calculated coupling because splitting is reduced by a scaling factor.<sup>66</sup> For the PISEMA MAS, the exact Hartmann–Hahn matching condition yields a maximum scaling factor of 0.816 ( $\sin 54.7^\circ$ ), although a perfect Hartmann–Hahn matching is not usually obtained because the scaling factor is lower. In the rigid system, the expected splitting value is approximately 18.5 kHz (22.7 kHz  $\times$  0.816). Fast molecular motion can reduce the principal component of the dipolar tensor by an order

parameter ranging from 0.5 to 1; the latter value represents a rigid system.<sup>67</sup>

The splitting values for the rigid parts of samples **1a**, **1b**, and **2** are in a range of 16.3–17.6 kHz. This range is lower than the theoretically predicted value because of Hartmann–Hahn imperfection. However, compared to the value for a rigid system, splitting that is decreased by approximately 5 kHz or more needs only to be explained by local molecular motion; the exact value of splitting depends on movement topology. The molecular dynamics of side chain C-end of amino acids and aromatic regions are evident for all samples. As an example, we show the position C54 of sample **1a** (Figure 6A) and position

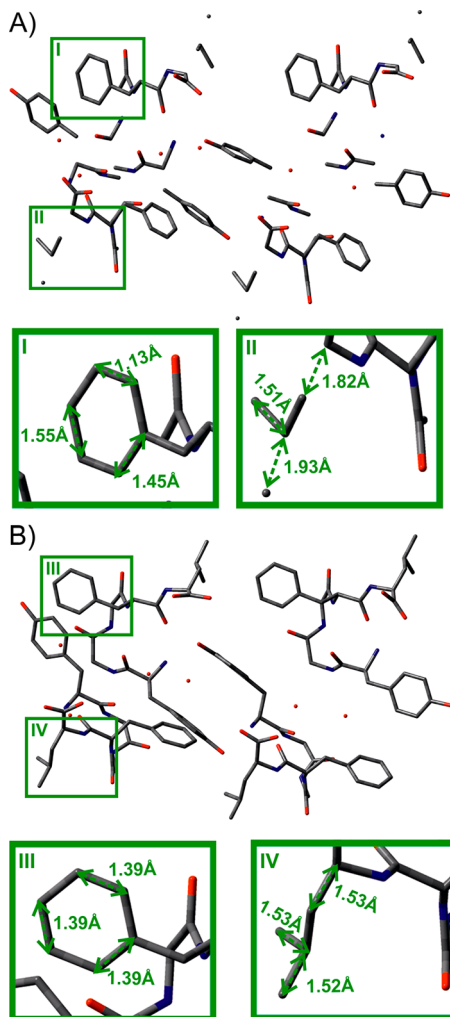


**Figure 12.** Comparison of X-ray (A) and the full optimized (B) structure **1a** with enlarged parts of both systems. Selected interatomic distances are indicated.

C15/17 of sample **1b** (Figure 6E). Two dipolar splittings for the resonance line representing carbon 54 are apparent. A similar conclusion is also valid for C15/C17. This indicates that such signals correspond to at least two different molecules with distinct molecular motions in the asymmetric unit cell.

(v) **Computation of the NMR Shielding Parameters and Correlation between Theoretical and Experimental Data.** As discussed previously, the X-ray data for the investigated enkephalins locate these compounds in the group of samples with significant molecular disorder. The *R*-factors are found to be 14.0 (**1a**), 8.9 (**1b**), and 10.5 (**2**). Special care must be taken in GIPAW calculations for such materials. In our project, the NMR shielding values were obtained under periodic boundary conditions using two models for each sample. First, the coordinates of heavy atoms deposited in the crystallographic database were used as an input file for GIPAW computing (model M1). Second, X-ray data were used to generate models with preserved geometry of the unit cell and optimized coordinates of heavy atoms and protons, which were then used for further calculations (model M2).<sup>68</sup> The calculated NMR shielding parameters are included in the Supporting Information.

Figures 7 and 8 show the correlations between experimental  $^{13}\text{C} \delta_{ii}$  and computed shielding  $^{13}\text{C} \sigma_{ii}$  NMR parameters for

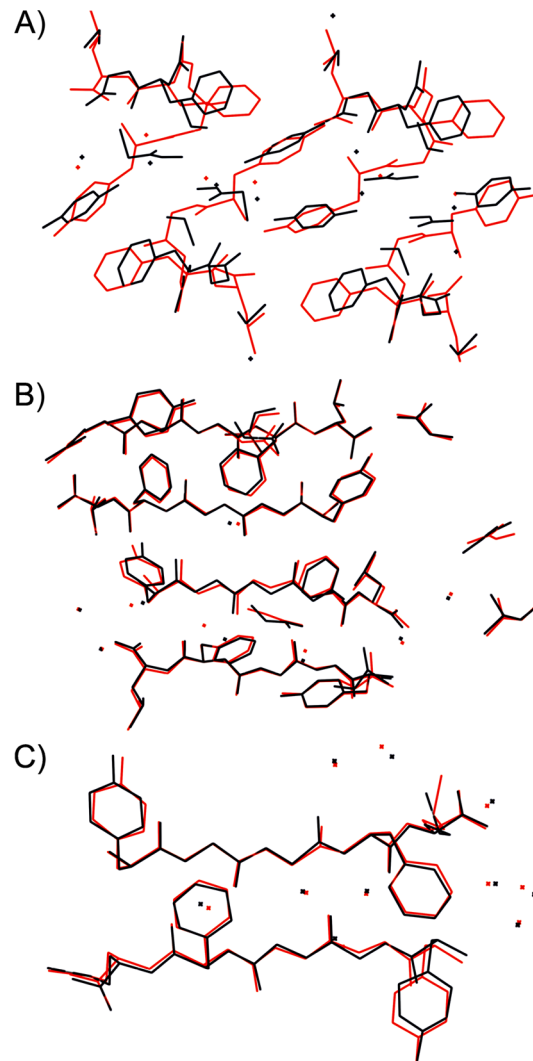


**Figure 13.** Overlap of the fully optimized structures **1a**, **1b**, and **2** according to the GIPAW approach (shown by the red stick model) and the structures before optimization (the black stick model). To clarify, only heavy atoms are shown.

both models. As we predicted, these correlations are very poor for model M1. The scatter of  $^{13}\text{C}$  CST points for sample **1a** (Figure 7A) is very large, and the establishment of regression and trends is not possible. The correlation between isotropic values  $^{13}\text{C} \delta_{iso}$  versus  $^{13}\text{C} \sigma_{iso}$  (Figure 7B) is slightly better but, again, is far from an acceptable trend. A similar tendency was observed for samples **1b** and **2**, even though the scatter of points was not as significant (see Supporting Information). The simple conclusions from this preliminary observation are that high *R*-factor values can be easily recognized in a  $^{13}\text{C} \delta_{ii}$ / $^{13}\text{C} \sigma_{ii}$  plot and that higher *R*-factor values generate increased scatter.

Much better correlations were obtained for model M2. Parts A, B, and C of Figure 8 show the plot of  $^{13}\text{C} \delta_{iso}$  versus  $^{13}\text{C} \sigma_{iso}$  for samples **1a**, **1b**, and **2**. As seen, the  $^{13}\text{C}$  isotropic values represent an almost perfect correlation with the intercept between 163.5 and 168.4 ppm and a slope that is very close to 1 for all peptides. The calculated  $^{13}\text{C}$  CST parameters show good agreement with the GIPAW calculated results for all investigated compounds (parts D, E, and F of Figure 8).

As we discussed above, the  $^{13}\text{C}$  CST and, consequently, the chemical shift anisotropy (CSA) parameters are influenced by

molecular dynamics. This phenomenon is not easily recognized in Figure 8 and is better observed when the span parameter expressed by the equation  $\Omega = \delta_{11} - \delta_{33}$  is analyzed. The plot of the experimental and calculated span  $\Omega$  values for **1a**, **1b**, and **2** enkephalins is displayed in Figure 9. For an ideal correlation, the slope is equal to 1 (represented by solid line in figures). It is apparent from the experimental span values for the phenyl ring of tyrosine, which is represented by C14–C18 carbons, as well as the phenyl rings of phenylalanine, which are represented by C44–C48, that the carbons do not fit the calculated data (Figure 9A) because of large-scale molecular dynamics. These results are very consistent with the PISEMA measurements discussed in section iv. Notably, local molecular motion is also seen in aliphatic regions for samples **1a** and **2**.

Further support for the correctness of our applied model is obtained from the correlation of proton chemical shifts with computed values. Figure 10 shows the appropriate correlations for all three samples calculated using model M2. As one can see, the  $R^2$  values are in range from 0.94 to 0.97. It is important to note that the indirect method of assigning proton chemical shifts may be a reason for this imperfect correlation.

(vi) **NMR Crystallography of Enkephalins.** The NMR data presented in the previous sections clearly demonstrate that the GIPAW-computed structures for samples **1a**, **1b**, and **2** better correlate with experimental parameters than those taken from X-ray studies. In fact, the coordinates for the GIPAW model M2 and the X-ray structure are significantly dissimilar. Figure 11 shows histograms presenting considerable differences between the positions of heavy atoms for all three samples. The biggest distinction is seen for sample **1a** (Figure 11A), which is represented by the highest value of  $R^2$ . Differences exceeding 1.5 Å mean that individual carbon atoms were wrongly assigned to the incorrect molecules in the crystallographic unit cells. This problem is illustrated in Figure 12.

The lack of consistency in the X-ray solution was apparent when we analyzed the structure of sample **1a**. Figure 12A shows the alignment of molecules in the unit cell. As seen with coordinates deposited in the CCDC, it is difficult to construct bonds between individual atoms. A deeper look into the structure displayed in zoom I and zoom II revealed that the lengths of carbon–carbon bonds are very different, which does not make physical and/or chemical sense. Figure 12B shows the same sample **1a** optimized via the GIPAW approach. The zoom III and zoom IV present the molecule with reasonable distances between carbon atoms that correlate very well with the aromatic ring bond lengths and single bond lengths reported in the literature. After geometric optimization, the unit cell is well organized, and it is possible to draw the proper alignment of molecules. GIPAW coordinates taken as inputs for calculations of NMR parameters support this very good consistency.

The results discussed here enable us to generate a new set of coordinates for the crystal structures of enkephalins **1a**, **1b**, and **2**. Figure 13 shows the unit cells for all three molecules. The black color reflects the X-ray geometry, while the red color indicates the conformation obtained using GIPAW. Inspection of the overlapped structures clearly reveals that the most substantial distinction is seen for sample **1a**, whereas for samples **1b** and **2**, the X-ray and GIPAW data are slightly different. The largest discrepancy is noted for aromatic residues and, in the case of **1b**, the main skeleton. These distinctions may be the result of dynamic processes in the crystal lattice, which influence the quality of X-ray refinement.

## CONCLUSIONS

In this paper, we present a methodology that allows for the fine refinement of crystal and molecular structures for compounds for which poor quality data are deposited in the crystallographic databases. The problem of molecular disorder in the crystal lattice may not be very common, but it is not marginal. In the Cambridge Crystallographic Data Center (CCDC), there are 22 000 deposited structures with  $R$ -factor values over 10 (3.5% of all X-ray structures). The enkephalins reported in this work belong to this group of compounds.

The methodology presented here is general and can be used for each crystalline sample possessing magnetically active spins that can be measured by solid-state NMR spectroscopy. Specifically, this approach is dedicated to organic and bioorganic compounds because  $^1\text{H}$ ,  $^{13}\text{C}$ ,  $^{15}\text{N}$ , and  $^{31}\text{P}$  nuclei with spin  $I = 1/2$  are easy to measure, and the results can be unambiguously interpreted. As we demonstrated, the comparative analysis of experimental and computed NMR parameters (isotropic chemical shifts and principal components of chemical shift tensor) immediately shows the quality of the refinement. Such analysis is also a good quality test for the chosen computational model.

Finally, we show that local molecular dynamics exert a strong influence on the chemical shift anisotropy but fortunately do not significantly disturb the position of atoms in the crystal lattice. This conclusion is consistent with recent papers of Dracinsky et al.<sup>69,70</sup> and Harper and co-workers.<sup>71</sup> As they revealed, atomic dynamics lead to apparent shortening of interatomic distances observed by diffraction but the effects of fast motions on structures are not expected to change significantly the relative positioning of signals in calculated NMR spectra.

Our work clearly proves that GIPAW-generated coordinates for all three enkephalins are reasonable and reflect the geometries of real samples.

## ASSOCIATED CONTENT

### S Supporting Information

$^1\text{H}$  spectra with signal assignments, F1 slices from PISEMA MAS NMR experiments, and correlations between NMR experimental data and calculated results; atomic coordinates of structures; tables with numerical results of quantum mechanical calculations; experimental chemical shifts. This material is available free of charge via the Internet at <http://pubs.acs.org>.

## AUTHOR INFORMATION

### Corresponding Authors

\*T.P.: e-mail, tpawlak@cbmm.lodz.pl.

\*M.J.P.: e-mail, marekpot@cbmm.lodz.pl.

### Notes

The authors declare no competing financial interest.

## ACKNOWLEDGMENTS

We thank Dr. Agata Jeziorna and Piotr Paluch for technical support. The authors are grateful to the Polish National Science Centre (NCN) for financial support under Grant 2011/01/N/ST4/03108. The computational resources were partially provided by the Polish Infrastructure for Supporting Computational Science in the European Research Space (PL-GRID) and ACK CYFRONET AGH grant MNiS-W/IBM\_BC\_HS21/CBMM PAN/029/2011.

## ■ REFERENCES

- (1) Waseda, Y.; Matsubara, E.; Shinoda, K. *X-Ray Diffraction Crystallography*; Springer: Heidelberg, Germany, 2011.
- (2) Harris, R. K.; Wasylissen, R. E.; Duer, M. J. *NMR Crystallography in Encyclopedia of Magnetic Resonance*; John Wiley & Sons Ltd.: New York, 2009.
- (3) Webber, A. L.; Emsley, L.; Claramunt, R. M.; Brown, S. P. NMR Crystallography of Campho[2,3-c]pyrazole ( $Z' = 6$ ): Combining High-Resolution  $^1\text{H}$ - $^{13}\text{C}$  Solid-State MAS NMR Spectroscopy and GIPAW Chemical-Shift Calculations. *J. Phys. Chem. A* **2010**, *114*, 10435–10442.
- (4) Webber, A. L.; Elena, B.; Griffin, J. M.; Yates, J. R.; Pham, T. N.; Mauri, F.; Pickard, C. J.; Gil, A. M.; Stein, R.; Lesage, et al. Complete  $(1)\text{H}$  Resonance Assignment of Beta-Maltose from  $(1)\text{H}$ - $(1)\text{H}$  DQ-DQ CRAMPS and  $(1)\text{H}$  (DQ-DUMBO)- $(13)\text{C}$  SQ Refocused INEPT 2D Solid-State NMR Spectra and First Principles GIPAW Calculations. *Phys. Chem. Chem. Phys.* **2010**, *12*, 6970–6983.
- (5) Harris, R. K.; Cadars, S.; Emsley, L.; Yates, J. R.; Pickard, C. J.; Jetti, R. K.; Griesser, U. NMR Crystallography of Oxybuprocaine Hydrochloride, Modification II°. *Phys. Chem. Chem. Phys.* **2007**, *9*, 360–368.
- (6) Salager, E.; Stein, R. S.; Pickard, C. J.; Elena, B.; Emsley, L. Powder NMR Crystallography of Thymol. *Phys. Chem. Chem. Phys.* **2009**, *11*, 2610–2621.
- (7) Salager, E.; Day, G. M.; Stein, R. S.; Pickard, C. J.; Elena, B.; Emsley, L. Powder Crystallography by Combined Crystal Structure Prediction and High-Resolution  $^1\text{H}$  Solid-State NMR Spectroscopy. *J. Am. Chem. Soc.* **2010**, *132*, 2564–2566.
- (8) Harris, R. K.; Hodgkinson, P.; Zorin, V.; Dumez, J.-N.; Elena-Herrmann, B.; Emsley, L.; Salager, E.; Stein, R. S. Computation and NMR Crystallography of Terbutaline Sulfate. *Magn. Reson. Chem.* **2010**, *48*, S103–S112.
- (9) Yates, J. R.; Dobbins, S. E.; Pickard, C. J.; Mauri, F.; Ghi, P. Y.; Harris, R. K. A Combined First Principles Computational and Solid-State NMR Study of a Molecular Crystal: Flurbiprofen. *Phys. Chem. Chem. Phys.* **2005**, *7*, 1402–1407.
- (10) Yates, J. R.; Pham, T. N.; Pickard, C. J.; Mauri, F.; Amado, A. M.; Gil, A. M.; Brown, S. P. Probing Intermolecular Crystal Packing in  $\Gamma$ -Indomethacin by High-Resolution  $(1)\text{H}$  Solid-State NMR Spectroscopy. *J. Am. Chem. Soc.* **2005**, *127*, 10216–10220.
- (11) Ośmiałowski, B.; Kolehmainen, E.; Ikonen, S.; Ahonen, K.; Lofman, M. NMR Crystallography of 2-Acylamino-6-[ $1\text{H}$ ]-Pyridones: Solid-State NMR, GIPAW Computational, and Single Crystal X-Ray Diffraction Studies. *J. Mol. Struct.* **2011**, *106*, 678–683.
- (12) Drašković, B. M.; Bogdanović, G. A.; Neelakantan, M. A.; Chamayou, A.-C.; Thalamuthu, S.; Avadhut, Y. S.; Schmedt Auf Der Günne, J.; Banerjee, S.; Janiak, C. *N*-O-Vanillylidene-L-Histidine: Experimental Charge Density Analysis of a Double Zwitterionic Amino Acid Schiff-Base Compound. *Cryst. Growth Des.* **2010**, *10*, 1665–1676.
- (13) Küçükbenli, E.; Sonkar, K.; Sinha, N.; De Gironcoli, S. Complete  $^{13}\text{C}$  NMR Chemical Shifts Assignment for Cholesterol Crystals by Combined CP-MAS Spectral Editing and ab Initio GIPAW Calculations with Dispersion Forces. *J. Phys. Chem. A* **2012**, *116*, 3765–3769.
- (14) Hušák, M.; Kratochvíl, B.; Jegorov, A.; Brus, J.; Maixner, J.; Rohlfíček, J. Simvastatin: Structure Solution of Two New Low-Temperature Phases from Synchrotron Powder Diffraction and SS-NMR. *Struct. Chem.* **2010**, *21*, 511–518.
- (15) Santos, S. M.; Rocha, J.; Mafra, L. NMR Crystallography: Toward Chemical Shift-Driven Crystal Structure Determination of the  $\beta$ -Lactam Antibiotic Amoxicillin Trihydrate. *Cryst. Growth Des.* **2013**, *13*, 2390–2395.
- (16) Pawlak, T.; Paluch, P.; Trzeciak-Karlikowska, K.; Jeziorna, A.; Potrzebowksi, M. J. Study of the Thermal Processes in Molecular Crystals of Peptides by Means of NMR Crystallography. *CrystEngComm* **2013**, *15*, 8680–8692.
- (17) Hughes, J.; Smith, T. W.; Kosterlitz, H. W.; Fothergill, L. A.; Morgan, B. A.; Morris, H. R. Identification of Two Related Pentapeptides from the Brain with Potent Opiate Agonist Activity. *Nature* **1975**, *258*, 577–580.
- (18) Simantov, R.; Snyder, S. H. Morphine-like Peptides in Mammalian Brain: Isolation, Structure Elucidation, and Interactions with the Opiate Receptor. *Proc. Natl. Acad. Sci. U.S.A.* **1976**, *73*, 2515–2519.
- (19) Lee, H.-K.; Smith, M. D.; Smith, B. J.; Grussendorf, J.; Xu, L.; Gillies, R. J.; White, H. S.; Bulaj, G. Anticonvulsant Met-Enkephalin Analogs Containing Backbone Spacers Reveal Alternative Non-Opioid Signaling in the Brain. *ACS Chem. Biol.* **2009**, *4*, 659–671.
- (20) Griffin, J. F.; Langs, D. A.; Smith, G. D.; Blundell, T. L.; Tickle, I. J.; Bedarkar, S. The Crystal Structures of [Met5]Enkephalin and a Third Form of [Leu5]Enkephalin: Observations of a Novel Pleated Beta-Sheet. *Proc. Natl. Acad. Sci. U.S.A.* **1986**, *83*, 3272–3276.
- (21) Karle, I. L.; Karle, J.; Mastropaoletti, D.; Camerman, A.; Camerman, N. [Leu5]Enkephalin: Four Cocrystallizing Conformers with Extended Backbones That Form an Antiparallel [Beta]-Sheet. *Acta Crystallogr.* **1983**, *B39*, 625–637.
- (22) Smith, G. D.; Griffin, J. F. Conformation of [Leu5]Enkephalin from X-ray Diffraction: Features Important for Recognition at Opiate Receptor. *Science* **1978**, *199*, 1214–1216.
- (23) Blundell, T. L.; Hearn, L.; Tickle, I. J.; Palmer, R. A.; Morgan, B. A.; Smith, G. D.; Griffin, J. F. Crystal Structure of [Leu5]Enkephalin. *Science* **1979**, *205*, 220.
- (24) Camerman, A.; Mastropaoletti, D.; Karle, I. L.; Karle, J.; Camerman, N. Crystal Structure of Leucine-Enkephalin. *Nature* **1983**, *306*, 447–450.
- (25) Mastropaoletti, D.; Camerman, A.; Camerman, N. Crystal Structure of Methionine-Enkephalin. *Biochem. Biophys. Res. Commun.* **1986**, *134*, 698–703.
- (26) Clark, S. J.; Segall, M. D.; Pickard, C. J.; Hasnip, P. J.; Probert, M. J.; Refson, K.; Payne, M. C. First Principles Methods Using CASTEP. *Z. Kristallogr.* **2005**, *220*, 567–570.
- (27) Segall, M. D.; Lindan, P. J. D.; Probert, M. J.; Pickard, C. J.; Hasnip, P. J.; Clark, S. J.; Payne, M. C. First-Principles Simulation: Ideas, Illustrations and the CASTEP Code. *J. Phys.: Condens. Matter* **2002**, *14*, 2717–2744.
- (28) Pickard, C. J.; Mauri, F. All-Electron Magnetic Response with Pseudopotentials: NMR Chemical Shifts. *Phys. Rev. B* **2001**, *63*, 245101.
- (29) Yates, J. R.; Pickard, C. J.; Mauri, F. Calculation of NMR Chemical Shifts for Extended Systems Using Ultrasoft Pseudopotentials. *Phys. Rev. B* **2007**, *76*, 024401.
- (30) Fung, B. M.; Khitrit, A. K.; Ermolaev, K. An Improved Broadband Decoupling Sequence for Liquid Crystals and Solids. *J. Magn. Reson.* **2000**, *142*, 97–101.
- (31) Antzutkin, O. N.; Shekar, S. C.; Levitt, M. H. Two-Dimensional Sideband Separation in Magic-Angle-Spinning NMR. *J. Magn. Reson., Ser. A* **1995**, *115*, 7–19.
- (32) Topspin, version 3.0; Bruker Biospin GmbH, Karlsruhe, Germany.
- (33) Dvinskikh, S. V.; Sandstrom, D. Frequency Offset Refocused PISEMA-Type Sequences. *J. Magn. Reson.* **2005**, *175*, 163–169.
- (34) Mao, K.; Wiench, J. W.; Lin, V. S.-Y.; Pruski, M. Indirectly Detected Through-Bond Chemical Shift Correlation NMR Spectroscopy in Solids Under Fast MAS: Studies of Organic-Inorganic Hybrid Materials. *J. Magn. Reson.* **2009**, *196*, 92–95.
- (35) Ishii, Y.; Tycko, R. Sensitivity Enhancement in Solid State  $^{15}\text{N}$  NMR by Indirect Detection with High-Speed Magic Angle Spinning. *J. Magn. Reson.* **2000**, *142*, 199–204.
- (36) Morcombe, C. R.; Zilm, K. W. Chemical Shift Referencing in MAS Solid State NMR. *J. Magn. Reson.* **2003**, *162*, 479–486.
- (37) Perdew, J. P.; Burke, K.; Ernzerhof, K. M. Generalized Gradient Approximation Made Simple. *Phys. Rev. Lett.* **1996**, *77*, 3865.
- (38) Vanderbilt, D. Soft Self-Consistent Pseudopotentials in a Generalized Eigenvalue Formalism. *Phys. Rev. B* **1990**, *41*, 7892.
- (39) Monkhorst, H. J.; Pack, J. D. On Special Points for Brillouin Zone Integrations. *Phys. Rev. B* **1976**, *13*, 5188.

- (40) Nocedal, J.; Wright, S. J. *Numerical Optimization*, 2nd ed.; Springer-Verlag: Berlin, NY, 2006.
- (41) Trzeciak-Karlikowska, K.; Bujacz, A.; Jeziorna, A.; Ciesielski, W.; Bujacz, G. D.; Gajda, J.; Pentak, D.; Potrzebowksi, M. J. Solid-State NMR and X-ray Diffraction Study of Structure and Dynamics of Dihydrate and Anhydrous Form of Tyr-Ala-Phe. *J. Cryst. Growth Des.* **2009**, *9*, 4051–4059.
- (42) Kamihira, M.; Naito, A.; Nishimura, K.; Tuzi, S.; Saito, H. High-Resolution Solid-State  $^{13}\text{C}$  and  $^{15}\text{N}$  NMR Study on Crystalline Leu- and Met-Enkephalins: Distinction of Polymorphs, Backbone Dynamics, and Local Conformational Rearrangements Induced by Dehydration or Freezing of Motions of Bound Solvent Molecules. *J. Phys. Chem. B* **1998**, *102*, 2826–2834.
- (43) Kamihira, M.; Naito, A.; Tuzi, S.; Saito, H. Phenyl Ring Dynamics of Enkephalin Molecules and Behavior of Bound Solvents in the Crystalline States by  $^2\text{H}$  NMR Spectroscopy. *J. Phys. Chem. A* **1999**, *103*, 3356–3363.
- (44) Brown, P. B. Probing Proton–Proton Proximities in the Solid State. *Prog. Nucl. Magn. Res.* **2007**, *50*, 199–251.
- (45) Brown, S. Applications of High-Resolution  $^1\text{H}$  Solid-State NMR. *Solid State Nucl. Magn. Reson.* **2012**, *41*, 1–27.
- (46) Chu, P.-J.; Potrzebowksi, M. J.; Scott, A. I.; Gao, Y. Conformational Studies of *N*-Benzoyl-L-Phenylalanine by Combined Rotation and Multiple-Pulse Spectroscopy Proton Nuclear Magnetic Resonance. *J. Am. Chem. Soc.* **1990**, *112*, 881–883.
- (47) Lange, A.; Scholz, I.; Manolikas, T.; Ernst, M.; Meier, B. H. Low-Power Cross Polarization in Fast Magic-Angle Spinning NMR Experiments. *Chem. Phys. Lett.* **2009**, *468*, 100–105.
- (48) Ernst, M.; Samoson, A.; Meier, B. H. Low-Power Decoupling in Fast Magic-Angle Spinning NMR. *Chem. Phys. Lett.* **2001**, *348*, 293–302.
- (49) Hediger, S.; Meier, B. H.; Ernst, R. R. Rotor-Synchronized Amplitude-Modulated Nuclear Magnetic Resonance Spin-Lock Sequences for Improved Cross Polarization under Fast Magic Angle Sample Spinning. *J. Chem. Phys.* **1995**, *102*, 4000–4011.
- (50) Caravatti, P.; Bodenhausen, G.; Ernst, R. R. Heteronuclear Solid-State Correlation Spectroscopy. *Chem. Phys. Lett.* **1982**, *89*, 363–367.
- (51) Caravatti, P.; Braunschweiler, L.; Ernst, R. R. Heteronuclear Correlation Spectroscopy in Rotating Solids. *Chem. Phys. Lett.* **1983**, *100*, 305–310.
- (52) Van Rossum, B.-J.; Foerster, H.; De Groot, H. J. M. High-Field and High-Speed CP-MAS  $^{13}\text{C}$  NMR Heteronuclear Dipolar-Correlation Spectroscopy of Solids with Frequency-Switched Lee–Goldburg Homonuclear Decoupling. *J. Magn. Reson.* **1997**, *124*, 516–519.
- (53) Zhou, D. H.; Rienstra, C. E. Rapid Analysis of Organic Compounds by Proton-Detected Heteronuclear Correlation NMR Spectroscopy with 40 kHz Magic-Angle Spinning. *Angew. Chem., Int. Ed.* **2008**, *47*, 7328–7331.
- (54) Mao, K. M.; Pruski, M. Directly and Indirectly Detected Through-Bond Heteronuclear Correlation Solid-State NMR Spectroscopy under Fast MAS. *J. Magn. Reson.* **2009**, *201*, 165–174.
- (55) Dixon, W. T. Spinning-Sideband-Free and Spinning-Sideband-Only NMR Spectra in Spinning Samples. *J. Chem. Phys.* **1982**, *77*, 1800–1809.
- (56) Pawlak, T.; Trzeciak-Karlikowska, K.; Czernek, J.; Ciesielski, W.; Potrzebowksi, M. J. Computed and Experimental Chemical Shift Parameters for Rigid and Flexible YAF Peptides in the Solid State. *J. Phys. Chem. B* **2012**, *116*, 1974–1983.
- (57) Robinson, M.; Haynes, P. D. Dynamical Effects in ab Initio NMR Calculations: Classical Force Fields Fitted to Quantum Forces. *J. Chem. Phys.* **2010**, *133*, 084109.
- (58) Cadars, S.; Lesage, A.; Pickard, C. J.; Sautet, P.; Emsley, L. Characterizing Slight Structural Disorder in Solids by Combined Solid-State NMR and First Principles Calculations. *J. Phys. Chem. A* **2009**, *113*, 902–911.
- (59) Schanda, P.; Meier, B. H.; Ernst, M. Accurate Measurement of One-Bond H–X Heteronuclear Dipolar Couplings in MAS Solid-State NMR. *J. Magn. Reson.* **2011**, *210*, 246–259.
- (60) Burum, D. P.; Ernst, R. R. Net Polarization Transfer via a J-Ordered State for Signal. *J. Magn. Reson.* **1980**, *39*, 163–168.
- (61) Morris, G. A.; Freeman, R. Enhancement of Nuclear Magnetic Resonance Signals by Polarization Transfer. *J. Am. Chem. Soc.* **1979**, *101*, 760–762.
- (62) Ramamoorthy, A.; Wei, Y.; Lee, D. K. PISEMA Solid-State NMR Spectroscopy. *Annu. Rep. NMR Spectrosc.* **2004**, *52*, 1–52.
- (63) Ramamoorthy, A.; Opella, S. J. Two-Dimensional Chemical Shift/Heteronuclear Dipolar Coupling Spectra Obtained with Polarization Inversion Spin Exchange at the Magic Angle and Magic-Angle Sample Spinning (PISEMAMAS). *Solid State Nucl. Magn. Reson.* **1995**, *4*, 387–392.
- (64) Yamamoto, K.; Ermakov, V. L.; Lee, D. K.; Ramamoorthy, A. PITANSEMA-MAS, a Solid-State NMR Method To Measure Heteronuclear Dipolar Couplings under MAS. *Chem. Phys. Lett.* **2005**, *408*, 118–122.
- (65) Wu, C. H.; Ramamoorthy, A.; Opella, S. J. High-Resolution Heteronuclear Dipolar Solid-State NMR Spectroscopy. *J. Magn. Reson., Ser. A* **1994**, *109*, 270–272.
- (66) Fu, R.; Tian, C.; Kim, H.; Smith, S. A.; Cross, T. A. The Effect of Hartmann–Hahn Mismatching on Polarization Inversion Spin Exchange at the Magic Angle. *J. Magn. Reson.* **2002**, *159*, 167–174.
- (67) Hong, M.; Yao, X.; Jakes, K.; Huster, D. Investigation of Molecular Motions by Lee–Goldburg Cross-Polarization NMR Spectroscopy. *J. Phys. Chem. B* **2002**, *106*, 7355–7364.
- (68) Dudenko, D. V.; Yates, J. R.; Harris, K. D.M.; Brown, S. P. An NMR Crystallography DFT-D Approach To Analyse the Role of Intermolecular Hydrogen Bonding and  $\pi$ – $\pi$  Interactions in Driving Cocrystallisation of Indomethacin and Nicotinamide. *CrystEngComm* **2013**, *15*, 8797–8807.
- (69) Dracinsky, M.; Bour, P. Vibrational Averaging of the Chemical Shift in Crystalline Alpha-Glycine. *J. Comput. Chem.* **2012**, *33*, 1080–1089.
- (70) Dracinsky, M.; Hodgkinson, P. A Molecular Dynamics Study of the Effects of Fast Molecular Motions on Solid-State NMR Parameters. *CrystEngComm* **2013**, *15*, 8705–8712.
- (71) Harper, J. K.; Iuliucci, R.; Gruber, M.; Kalakewich, K. Refining Crystal Structures with Experimental  $^{13}\text{C}$  NMR Shift Tensors and Lattice-Including Electronic Structure Methods. *CrystEngComm* **2013**, *15*, 8693–8704.